Received: 4 June 2019 | Revised: 4 July 2019 | Accepted: 6 July 2019

DOI: 10.1002/er.4759

RESEARCH ARTICLE

WILEY INTERNATIONAL JOURNAL OF ENERGY RESEARCH

A comparative study of lumped equivalent circuit models of a lithium battery for state of charge prediction

Hongbin Ren | **Yuzhuang Zhao** | **Sizhong Chen** | **Lin Yang**

School of Mechanical Engineering, Beijing Institute of Technology, Beijing 100081, China

Correspondence
Yuzhuang Zhao, School of Mechanical Engineering, Beijing Institute of Technology. Beijing 100081, China.
Email: zyz1112@163.com

Funding information
National Key R&D Program of China, Grant/Award Number: 2017YFB0102600; National Natural Science Foundation of China, Grant/Award Number: 51605020

Summary

Battery modeling plays an important role in remaining range prediction and battery management system development. An accurate and realistic battery model is essential to design an efficient electric storage system. The goal of this paper is to investigate the performance of different circuit topologies for diffusion process in the equivalent circuit models (ECMs). The theory of diffusion process approximation by using resistive-capacitor (RC) networks is explained in frequency domain. The terminal voltage predictive capabilities of the ECMs are compared and validated with test data. The numerical simulation results show that model prediction accuracy and computation burdens increase along with the number of RC pairs. The ECM with three RC networks is the best choice in terms of the balance between accuracy and complexity for ternary lithium batteries. In addition, a novel method of combining unscented Kalman filter (UKF) algorithm with initial state of charge (SOC) acceleration convergence for SOC estimation is proposed. The results of urban dynamometer driving schedule (UDDS) show that ECM with three RC networks has the best comprehensive performance on calculation cost and SOC estimation accuracy.

KEYWORDS

battery modeling, ECMs, initial SOC correction acceleration, Li-ion battery, state of charge prediction

1 | INTRODUCTION

To reduce fossil fuel consumption and carbon footprint from ground transportation industry, drivetrain electrification is a promising alternative to conventional vehicle architecture. Hybrid electric vehicle or electric vehicle (HEV/EV) performance depends strongly on the performance of the battery pack. Li-ion batteries have lots of advantages in terms of power and energy density, efficiency, lower self-discharge, and lower maintenance; however, they also have several limitations: cost, high temperature sensitivity, and aging in function of usage.[1] An advanced battery management system (BMS) for temperature, power management, and aging prediction is essential to operate safely at maximum performance and avoid the weak points. The performance of BMS is heavily dependent on the knowledge of battery model and its dynamic response.[2,3]

The precision and complexity of ECMs are significant for SOC and SOH prediction in BMS.[4] The most commonly used battery modeling techniques can be grouped into two main categories[5]: physical-based electrochemical models[6,7] and semi-empirical equivalent circuit models (ECMs).[8-10] For physical-based Li-ion battery models, poor knowledge about the parameters of internal battery chemistry and high computational load often make it unpractical for engineering applications.[8] ECMs are widely used in architecture design of EV/HEV and BMS owing to its low calculation burden and high prediction capability.[9] The simplest ECM is composed of a resistance

in series with the ideal voltage source. This model is sufficient for fuel consumption and performance analysis of full vehicle, but not for advanced xEV applications, such as SOC/SOH estimation design. The advanced ECM can be used for dynamic simulation that considers intrinsic polarization process of the battery.[10] Both of instantaneous and non-instantaneous response to a change in input current can be captured in advanced ECM by utilizing the battery internal impedance including ohmic effect, charge transfer, and diffusion effects.[11] Usually, temporal and frequency domain testing are used for ECMs parameters identification. For time domain test, hybrid pulse power characterization (HPPC) is comprehensively used to identify the parameters for ECMs. A well-known technique for parameters' identification method for ECMs is recursive least squares (RLS) and its variations.[12,13] For frequency domain test, electrochemical impedance spectroscopy (EIS) measurements are utilized to obtain these parameters of ECMs.[14] Khalid et al[15] proposed impedance analyzer and Bayesian network method to fit the parameters of the ECM circuit elements.

In most existing studies of battery modeling, ECMs are widely used in Li-ion battery application. As we all know, the precision and calculation burden highly rely on the model parameters and structures. Genetic algorithm (GA),[16] particle swarm optimization (PSO),[17] the least-squares method, etc are widely used for parameters identification. However, the structures of ECMs, especially for the relationship between the number of R//C parallel and slow diffusion description precision, is seldom studied. For example, if the diffusion voltage drop is ignored because of battery impedance defined in high frequency range, the terminal voltage will be underestimated after long time charge or discharge. If the battery impedance is defined as the total low frequency impedance, the terminal voltage drop of the model will be overestimated during a dynamic cycle with short charge or discharge peaks. Therefore, the performance of different circuit topologies of diffusion process is an important factor for battery model accuracy.

The battery modeling by using ECMs and its application in SOC estimation are involved, and some contributions of this paper are made as follows: (a) A comparative study of the different number RC circuits in series are carried out; (b) the theory of diffusion model approximated by pairs of RC networks in series is clearly explained; (c) time and frequency domain analysis are used for battery model precision evaluation; and (d) the accuracy and computational load performance are studied in SOC estimation by using the unscented Kalman filter (UKF) method. The observed results of SOC are compared and validated under different circuit topologies and working conditions. Battery modeling and parameter identification are described in Section 2. The precision analysis in time and frequency domain is described in Section 3, and the SOC estimation based on UKF is outlined in Section 4. Some interesting conclusions are drawn in Section 5.

2 | BATTERY MODELING AND PARAMETER IDENTIFICATION

A cell's terminal voltage will depart away from open circuit voltage (OCV) during charging/discharging because of polarization phenomenon. Similarly, terminal voltage will converge to OCV when the current load is abruptly removed. As shown in Figure 1, the polarization, ie, electrochemical kinetic properties of ohmic resistance, charge transfer, and diffusion effects can be easily observed as a segment with zero imaginary part, semicircle, and Warburg semi-straight line in a Nyquist plot of a cell's EIS. EIS is an accurate analytical technique to obtain critical electrochemical parameters of battery including internal resistance, battery lifetime, and reaction kinetics and electrochemical mechanisms. The EIS was measured by the Solartron 1260A, and the alternating current (AC) response from the cell over a range of applied frequencies is analyzed and the impedance is calculated. The first one in ultra-high frequency impedance is ohmic resistances, which are contributed by electrolyte, separator, current collector, and electric conductivity of the active material. The second one is a semi-circular loop in mid-range frequencies caused by charge-transfer and double layer capacity occurred after a time delay. The last one, diffusion effect, is voltage response during rest period after discharging at the ultra-low frequency range. The frequency-dependent Warburg impedance $Z(jw) = 1/Y_0\sqrt{(jw)}$ (a 45° half line) is a constant phase element (CPE) that can describe the diffusion process of lithium ion batteries.[18] Mu et al[19] proposed fractional-order differential equation to describe the CPE, and this method can increase the precision at the expense of increasing the complexity and nonlinearity of the battery model. There is no simple equivalent circuit representation of a Warburg impedance, but it can be approximated by using n pairs of R//C in series.[20]

The accuracy of diffusion process of ECMs depends on the number pairs of R//C loops. With the increasing number of R//C parallel, the ECMs better fits the 45° half line of Warburg impedance in the Nyquist plane; however, the complexity and CPU processing time will also increase.[21]

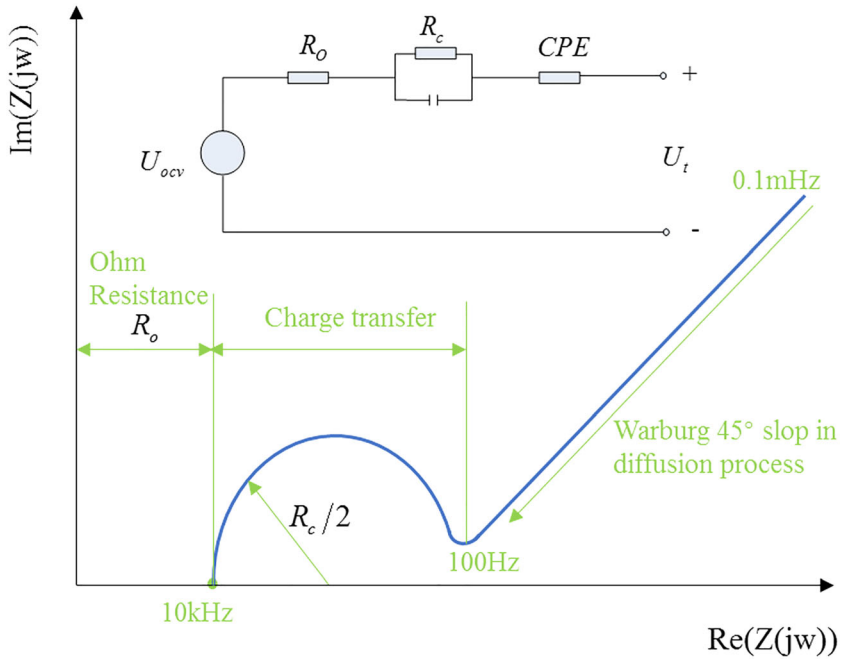

FIGURE 1 Ideal EIS plot for Li-ion battery and corresponding circuit [Colour figure can be viewed at wileyonlinelibrary.com]

During the discharge, the dynamic voltage drops caused by three parts including ohmic drop IR_o, charge transfer drop U_c, and diffusion drop described by CPE U_{CEP}. So the terminal voltage can be calculated by

$$U_t = U_{ocv} - IR_o - U_c - U_{CEP}, \tag{1}$$

where U_t is the terminal voltage of cell and I is the battery current. Here, current is positive when discharging; the ohmic resistance is the function of SOC, cell's temperature, and the passage of current; ie, $R_o = R_o(I,T,S)$. Two resistances, R_{ohmc} and R_{ohmd} are used to represent the charge and discharge ohmic resistance, respectively.

$$R_o = \begin{cases} R_{ohmc} & I < 0 \\ R_{ohmd} & I > 0 \end{cases} \tag{2}$$

The ohmic zone can be captured by steep charge and discharge current pulses in HPPC test. And the ohmic resistances are identified by the comparison between experimental voltage variation ΔU and current variation ΔI; ie,

$$R_o = \frac{\Delta U}{\Delta I}. \tag{3}$$

The identification results of ohmic resistance are determined by the sampling time of HPPC test, because the ohmic effect occurred in microsecond, and less than a sampling interval.

The charge transfer dynamics as a semi-cycle in EIS can be modeled as a single R//C pair.

$$C_c \frac{dU_c}{dt} = i - \frac{U_c}{R_c}, \tag{4}$$

where U_c is voltage drop caused by charge transfer and R_c and C_c are charge transfer resistance and capacitance, respectively.

The transfer function of Equation (4) is

$$\frac{U(s)}{I(s)} = \frac{R_c}{1 + C_c R_c s}, \tag{5}$$

where s is a complex number frequency parameter and Equation (5) can be considered as a general first-order transfer function.

The low frequency diffusion can be modeled by a non-integer order impedance, CPE, which is defined in frequency domain,

$$CPE(jw) = \frac{1}{Y_0(jw)^n} = \frac{1}{Y_0 w^n} e^{-n\frac{\pi}{2}j} (0 \le n \le 1), \tag{6}$$

where Y_0 is the CPE coefficient, n is the non-integer order of CPE, and j the is the imaginary unit. The phase of CPE is always constant as $-n\pi/2$; especially, $n = 1$ describes an ideal capacitor while the case $n = 0$ is a pure ohmic resistor, and n = 1/2 is an ideal Warburg impedance. And the slop of Warburg in Bode plot is −10 dB/dec. It can be proven that any equivalent circuit of CPE can be approximated by using RC element.[22,23] A typical Bode plot of single R//C network is shown in Figure 2; we can find that in low frequency, ie, left side of break point (0.1 Hz), the slop is 0 dB/dec, and in high frequency, the slop is −20 dB/dec. Thus, the −10 dB/dec for diffusion in low frequency can be piece-wisely approximated by the mid-frequency segments that are around the brake points, as shown in Figure 3. And the

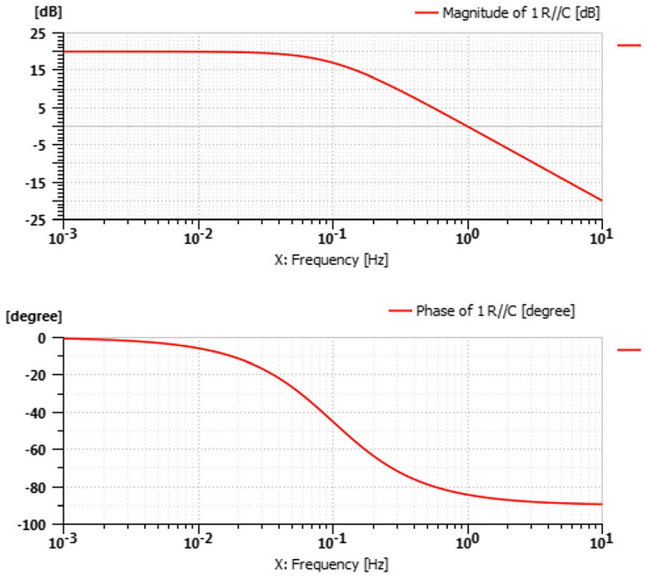

FIGURE 2 A typical Bode plot of single R//C network (the brake point is 0.1 Hz, $R = 10\ \Omega$) [Colour figure can be viewed at wileyonlinelibrary.com]

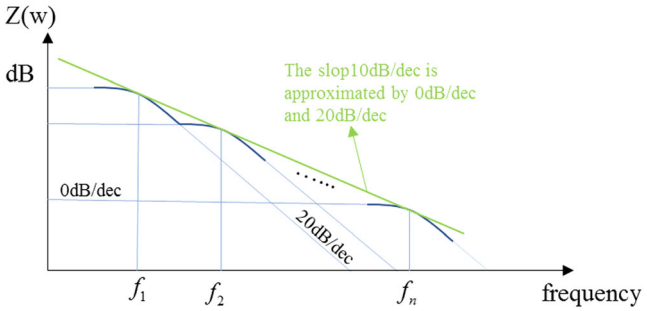

FIGURE 3 Piecewise approximation for −10 dB/dec by 0 and 20 dB/dec [Colour figure can be viewed at wileyonlinelibrary.com]

−10 dB/dec slop can be obtained by the transfer function presented in Figure 4, ie, n pairs of R//C networks in parallel, but this is not the only method to achieve. Figure 5 presented an example for the −10 dB/dec slop approximations by employing several first-order delays with

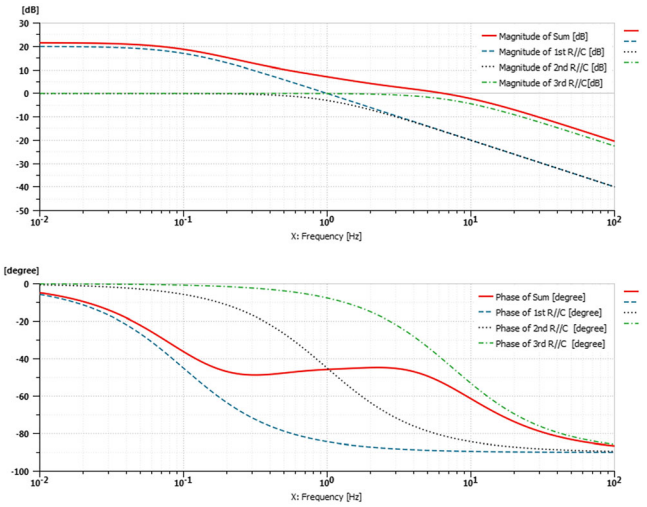

FIGURE 5 Bode plots comparison of first-order delay with different break points ($f_1 = 0.1$ Hz [blue dash-dot] and $f_2 = 1$ Hz [dotted black], and $f_3 = 10$ Hz [green dashed]) and corresponding in series (solid red) [Colour figure can be viewed at wileyonlinelibrary.com]

different break points. It can be found that in the frequency range of 0.1–10 Hz, the slop is close to −10 dB/dec, and the phase angle of transfer function is almost constant as 45°.

Thus, the diffusion voltage can be calculated by

$$U_p = \sum_{n=1}^{N} R_p^n \left(i - C_p^n \frac{dU_p^n}{dt} \right), \tag{7}$$

where U_p is the diffusion voltage drop and C_{pk} and R_{pk} are nth capacitor and resistive elements in equivalent circuit, respectively.

The differential equation of SOC can be written as

$$\frac{dS}{dt} = \eta \frac{i}{36Q}, \tag{8}$$

where S denotes the state of charge; η is the columbic efficiency, and the coulombic efficiency of lithium-ion battery is normally better than 99%; Q is the nominal

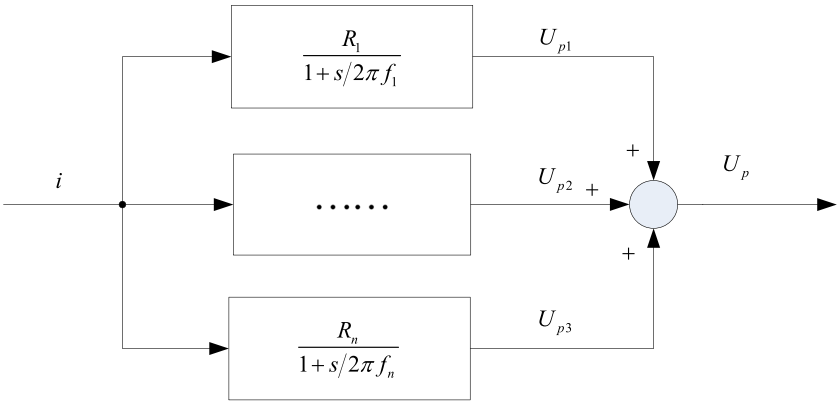

FIGURE 4 The transfer function implementation for −10 dB/dec (the brake points are $f1$,fa,...,fn) [Colour figure can be viewed at wileyonlinelibrary.com]

capacity of battery; the real capacity should be corrected according to the temperature and battery aging condition in battery SOC estimation algorithm.

3 | MODEL ACCURACY ASSESSMENT

As proven in Section 2, the diffusion process can be reproduced by employing multiple RC circuit in series. And different topology of RC parallel for ECMs is investigated and compared in the aspects of modeling complexity and precision, as shown in Figure 6. To validate the performance of the ECMs, the ternary Li(NiCoMn) battery is used. The battery nominal capacity is 2.3 Ah, with 4.2 and 2.7 V maximum and cut-off voltages, respectively.

The voltage response of hybrid pulse power characterization (HPPC) test in time domain is used to assess the relationship between OCV and SOC and corresponding RC parameters. Firstly, the rest zones are recognized to determine the OCV-SOC curve. Steep charge and discharge current variations are used to capture the ohmic effects in the experimental data, and the charging and discharging resistance can be identified by the ratio between voltage and current variation. The charge transfer and diffusion RC parameters in ECMs can be identified by fitting the voltage converging data.

Figure 7 depicted the HPPC test profile and corresponding SOC of the battery. The 3 C, 6 C, and 10 C charging and discharging pulse current are carried out in the test. The impact of current ripple on battery internal resistance can thus be considered in ECMs. The time history of terminal voltage comparison between experimental data and ECMs with different circuit topologies of diffusion process are presented in Figure 8, and a close

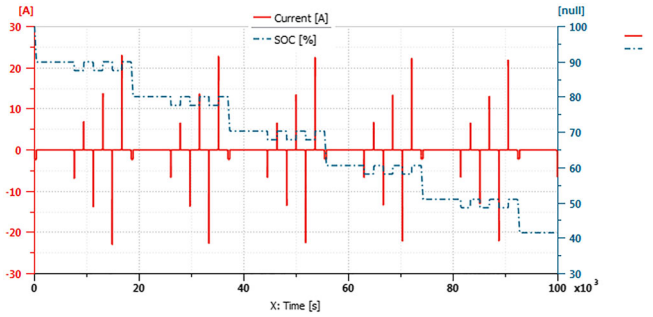

FIGURE 7 Experiment current and battery SOC at $T = 25°$ [Colour figure can be viewed at wileyonlinelibrary.com]

for short and long current pulse are plotted in Figure 9. During the rest zone and ohmic process, the fitting error is almost close to 0; this means that EMCs are with high accuracy during rest and high frequency ohmic process thanks to the high-fidelity model of OCV and identified charging and discharging ohmic impedance. For diffusion zone including electrochemical polarization and concentration polarization in low frequency zone, as shown in Figure 9, three types of models are presented with different fitting performance. A higher order ECM with RC parallel network could increase the precision in both pulse and relaxation voltage. However, when the order of ECM is more than 3, the computational expense and modeling complexity will increase significantly with limited accuracy increase according to the model error and CPU time analysis in Table 1, and this often makes the model unpractical in engineering applications.

Figures 10 and 11 present the spectra comparison with different topologies of ECM at 25° and 0°, respectively. It can be concluded that the 3RC ECM and 5RC's are close to 45° half line in low frequency in diffusion fitting compared with 1RC ECM. This is because

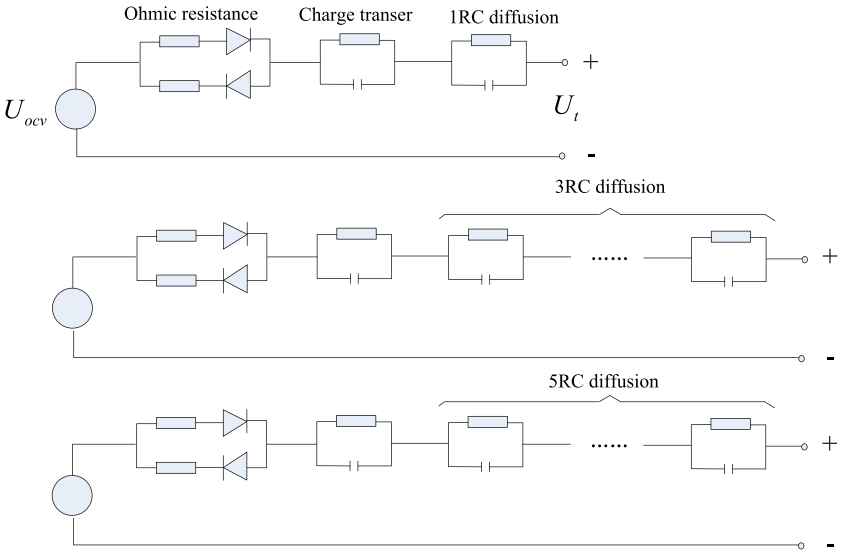

FIGURE 6 ECMs with different circuit topologies for diffusion process description [Colour figure can be viewed at wileyonlinelibrary.com]

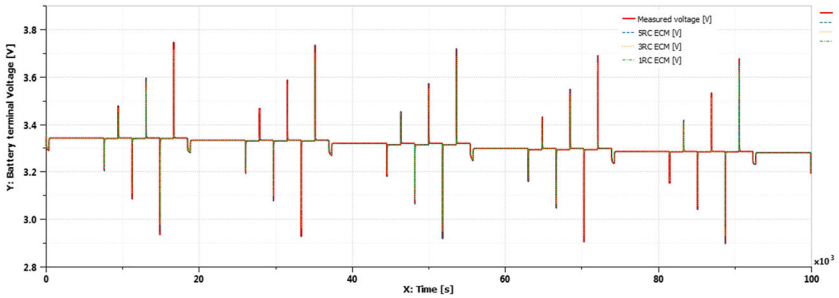

FIGURE 8 Model accuracy assessment for the 1RC (black dash-dot), 3RC (yellow dot), and 5RC (blue dashed) ECMs and corresponding measurement terminal voltage (solid red) [Colour figure can be viewed at wileyonlinelibrary.com]

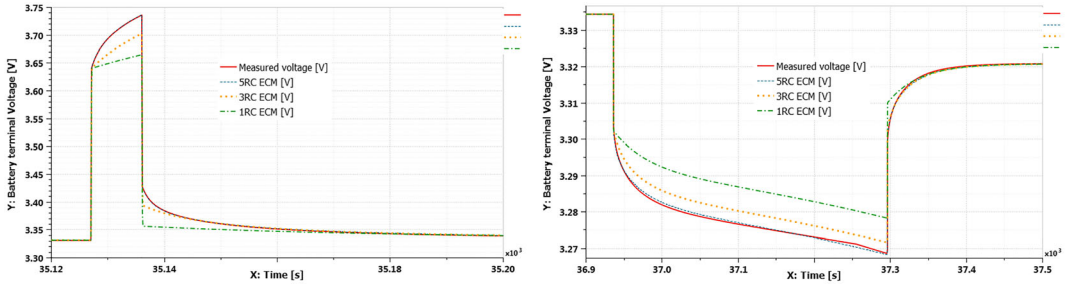

FIGURE 9 Close-up of three ECMs simulation results for short and long current pulse. Line styles and colors are the same as in Figure 8 [Colour figure can be viewed at wileyonlinelibrary.com]

TABLE 1 Model error analysis and calculation time comparison

	1RC Model		3RC Model		5RC Model	
Temperature	**25°**	**0°**	**25°**	**0°**	**25°**	**0°**
Max error[a], mV	57.5	86.7	22.5	34.2	18.6	30.1
Mean error, mV	18.05	27.32	9.21	13.37	7.34	11.25
CPU time[b], s	7.98		11.76		23.37	

[a]The maximum errors occurred at 10 C pulse.

[b]The simulation time is 100 000 s.

each RC pair can fit one semicircle, and any shape curve can be approximated by multiple RC parallel networks in Nyquist plane. Compared impedance spectra at high and low temperature, it is evident that with the

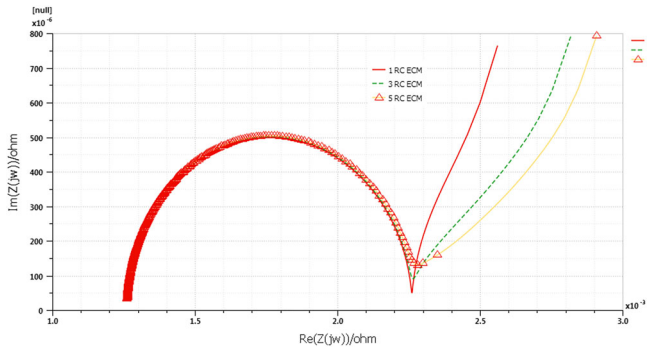

FIGURE 10 Impedance spectra comparison with different topologies of ECM at 25° [Colour figure can be viewed at wileyonlinelibrary.com]

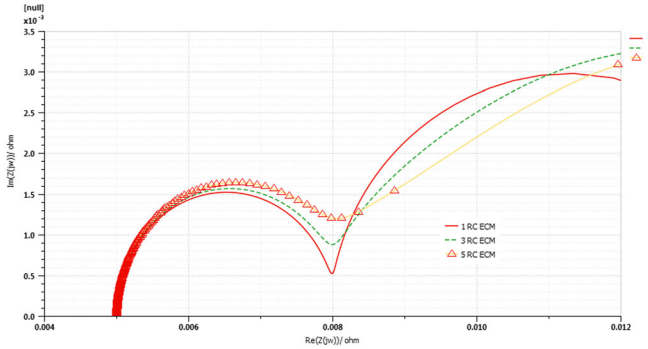

FIGURE 11 Impedance spectra comparison with different topologies of ECM at 0° [Colour figure can be viewed at wileyonlinelibrary.com]

decreasing of temperature, the semicircle in Nyquist plane moves to right side; ie, lower temperature increase the battery internal resistive properties due to the kinetic activity of electrochemistry and diffusivity reduction. The impaction of different SOCs to the impedance spectra are depicted in Figure 12. It can be distinguished that impedance spectra with lower SOC in Nyquist plane presents higher internal resistance.

4 | ECM-BASED SOC ESTIMATION

Battery management system (BMS) is significant for battery lifespan extension and ensuring that the battery will operate within the manufacturer specifications. And SOC

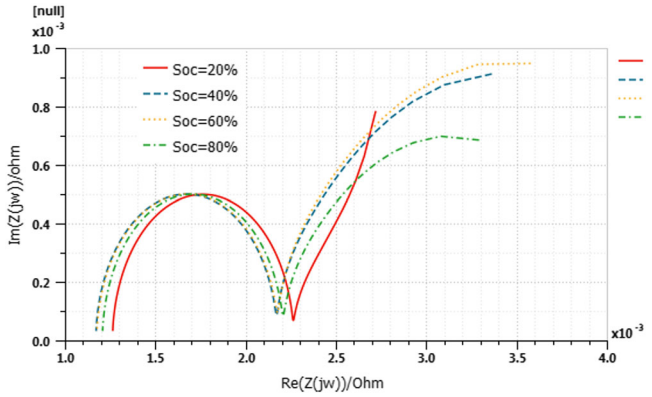

FIGURE 12 Impedance spectra comparison of 3RC ECM at different SOCs [Colour figure can be viewed at wileyonlinelibrary.com]

prediction is an important function of BMS. Accurate SOC estimation could determine the available energy, power limits, preventing damage and abuse, as well as charge balance etc. There are commonly two types of methods for SOC estimation, open-loop and close-loop. Current-based method, ie, coulomb counting, is open-loop type, and this method is low robust for initial SOC value and measurement noise. Model-based methods use sensor measurements and battery model to predict and correct the internal hidden states by the designed estimation algorithm. The estimator-based Kalman filter (KF) could produce an optimal solution to the continuous or discrete estimation problems. In this section, to compare and validate three different topologies ECMs, an unscented (sigma points) Kalman filter with initial SOC correction algorithm is presented. The estimation performance is much better than extended Kalman filter (EKF) at almost same computational cost. The UKF steps are listed in Table 2.

The continuous-time system can be discrete according Taylor first-order approximation with sampling time ΔT,

$$U_{p,k+1} = \sum_{n=1}^{N} \left\{ \frac{\Delta T}{C_{pk}^{n}} i_k + \left(1 - \frac{\Delta T}{R_{pk} C_{pk}^{n}}\right) U_{p,k}^{n} \right\}, \quad (9)$$

$$U_{t,k+1} = U_{o,k}(s_k) - i_k R_{o,k} - U_{p,k}, \quad (10)$$

$$S_{k+1} = S_k - \eta \frac{i}{36Q} \Delta T, \quad (11)$$

where N is the total number of RC network in series.

The UKF methods propagate the statistic through the nonlinear state function by utilizing the sigma-point approach at each sampling time step. The sigma-point can be designed by the symmetrically sampling method,

TABLE 2 Computation procedures of the UKF algorithm

a. Initialization step,

$\mathbf{x}_0 = E[\mathbf{x}_0]$, $\mathbf{P}_0$, $\mathbf{Q}$, $\mathbf{R}$

where $\mathbf{P}_0$ is initial error covariance; $\mathbf{Q}$ is the process noise covariance, ie, modeling error; and $\mathbf{R}$ is the measurement noise covariance. If one prefers to prior estimation results from model prediction, choose smaller value of $\mathbf{Q}$; similarly, if prefers to measurement from sensors, choose smaller value of $\mathbf{R}$.

b. The prior state estimate sigma vectors are computed by

$\chi_{k+1} = \chi_k + f(\chi_k, u_{k+1}, \mathbf{w}_{k+1}) \cdot \Delta T$, (1)

where $f(\cdot)$ is the mathematical model of the system; u_{k+1} is input; $\mathbf{w}_{k+1}$ is the process noise; and it is a white Gaussian noise with covariance $\mathbf{Q}$.

c. Output estimate is updated by

$\mathbf{Y}_{k+1} = h(\chi_{k+1}, u_{k+1}, \mathbf{v}_{k+1})$, (2)

where $h(\cdot)$ is system output; v_{k+1} is sensor noise with covariance R.

The prior state vector $\mathbf{x}_{k+1}$ and output $\mathbf{y}_{k+1}$ can be calculated by weighted sample mean of the sigma vectors

$$\begin{aligned} \mathbf{x}_{k+1|k} &\approx \sum_{i=1}^{2N+1} \left(W_i^m (\chi_{k+1})_i\right) \\ \mathbf{y}_{k+1} &\approx \sum_{i=1}^{2N+1} \left(W_i^m (Y_{k+1})_i\right) \end{aligned} \quad (3)$$

d. Error covariance update

The covariance of the state and output vector can be updated by

$$\begin{aligned} \mathbf{P}_{k+1|k}^{\mathbf{x}} &= \sum_{i=1}^{2N+1} \left[\mathbf{W}_i^c \left((\chi_{k+1})_i - \mathbf{x}_{k+1}\right)\left((\chi_{k+1})_i - \mathbf{x}_{k+1}\right)'\right] + \mathbf{Q} \\ \mathbf{P}_{k+1}^{\mathbf{y}} &= \sum_{i=1}^{2N+1} \left[\mathbf{W}_i^c \left((Y_{k+1})_i - \mathbf{y}_{k+1}\right)\left((\mathbf{Y}_{k+1})_i - \mathbf{y}_{k+1}\right)'\right] + \mathbf{R} \\ \mathbf{P}_{k+1}^{\mathbf{xy}} &= \sum_{i=1}^{2N+1} \left[\mathbf{W}_i^c \left((\chi_{k+1})_i - \mathbf{x}_{k+1}\right)\left((\mathbf{Y}_{k+1})_i - \mathbf{y}_{k+1}\right)'\right] \end{aligned} \quad (4)$$

The weight matrix can be computed by

$$\mathbf{W}_i^m = \left[\underbrace{\sigma/(L+\sigma), 1/2/(L+\sigma), \cdots, 1/2/(L+\sigma)}_{2N}\right] \quad (5)$$

$$\mathbf{W}_i^c = \left[\underbrace{\sigma/(L+\sigma) + 1 - \alpha^2 + \eta, 1/2/(L+\sigma), \cdots, 1/2/(L+\sigma)}_{2N}\right] \quad (6)$$ where

η considers the high order prior distribution and $\eta = 2$ is optimal for Gaussian distribution.

e. Estimation gain matrix calculation and state vector correction

$$\begin{aligned} \mathbf{K}_{k+1} &= \mathbf{P}_{k+1}^{xy} \left(\mathbf{P}_{k+1}^{y}\right)^{-1} \\ \mathbf{x}_{k+1|k+1} &= \mathbf{x}_{k+1|k} + \mathbf{K}_{k+1}\left(\mathbf{z}_{k+1} - \mathbf{y}_{k+1}\right) \\ \mathbf{P}_{k+1|k+1}^{x} &= \mathbf{P}_{k+1|k}^{x} - \mathbf{K}_{k+1} \mathbf{P}_{k+1}^{y} \left(\mathbf{K}_{k+1}\right)' \end{aligned} \quad (7)$$

where $\mathbf{z}_{k+1}$ is sensor measurements.

$$\chi_k = \begin{cases} \overline{\mathbf{x}} & k = 0 \\ \overline{\mathbf{x}} + \left(\sqrt{(L+\sigma)\mathbf{P}^{\mathbf{x}}}\right)_k & k = 1, 2, \cdots, n, \\ \overline{\mathbf{x}} - \left(\sqrt{(L+\sigma)\mathbf{P}^{\mathbf{x}}}\right)_{k-n} & k = n+1, \cdots, 2n \end{cases} \quad (12)$$

where the sigma points χ_k are designed as a set of $2n+1$ vector; $\mathbf{x}$ is system state vector in the observation

algorithm, the mean of χ_k is $\bar{\mathbf{x}}$, and the covariance of χ_k is $\mathbf{P}^{\mathbf{x}}$; L is the length of the state vector $\mathbf{x}$; σ is scaling parameter for χ_k; it can be described by the following equation[24]:

$$\sigma = \alpha^2(L + \kappa) - L, \tag{13}$$

where α is a constant value ($10^{-4} \leq \alpha \leq 1$), which determines the spread of the sigma points around $\bar{\mathbf{x}}$; L is the length of state vector $\mathbf{x}$; $\kappa \geq 0$; it keeps the covariance matrix positive definite.

Here, we choose $\mathbf{x} = [U_p \quad U_t \quad S]^T$ as state vector, choose current as system input, and choose terminal voltage as measurement. The sketch diagram of the SOC estimation is shown in Figure 13.

To enhance the convergence speed when the initial SOC deviates largely from true value, a simple but effective acceleration method is presented. During the first few iterations, if the measured terminal voltage is larger than the OCV from tabulated value according to estimated SOC, then the initial SOC is smaller than the true value, so the estimated SOC should be corrected by the acceleration convergence method, ie,

$$S_{k+1} = S_k + K_s(U_t - OCV) \quad \rightarrow \text{if } U_t - OCV > 0, \tag{14}$$

where K_s is correction gain for first few iterations.

The battery parameters can be identified offline by using the least square method. Three different topologies of ECMs are employed to SOC prediction based on designed UKF algorithm presented above. The performance including estimation precision and algorithm computational burden with different topologies of ECMs is investigated under nine consecutive UDDS drive cycles for typical city driving condition. The current load profiles are shown in Figure 14.

The actual initial SOC is unknown in practical application. Here, we assume that the value of initial SOC deviation from the true value is 5%, and the comparison of initial SOC convergence performance and error analysis between with and without converge acceleration technical are presented in Figure 15. It can be clearly found that with the initial SOC acceleration algorithm, the estimated SOC value can be converged within 20 seconds, while the converge time without initial SOC acceleration technique is around 800 seconds according to error analysis in Figure 15B. So the conclusion is that with initial SOC correction method, the convergence speed could be improved significantly.

The comparison of SOC estimation and errors analysis of three different ECMs under UDDS is plotted in Figure 16. It is easy to be found that the estimation errors based on both ECM with 3RC and 5RC networks are within 1% in whole time history, but the error from estimator based on the ECM with 1RC network is relatively larger. This is because the diffusion process cannot well be modeled precisely by just 1RC network in low frequency. The reason for SOC estimation error of 3RC and 5RC ECMs is mainly from modeling uncertainties and measurement noises; this can be further improved by online and offline parameters tuning in hardware-in-loop test. The maximum and mean errors of the SOC estimation as well as simulation time are shown in Table 3. According to the data analysis presented in Table 3, the performance of SOC estimator based on 3RC and 5RC

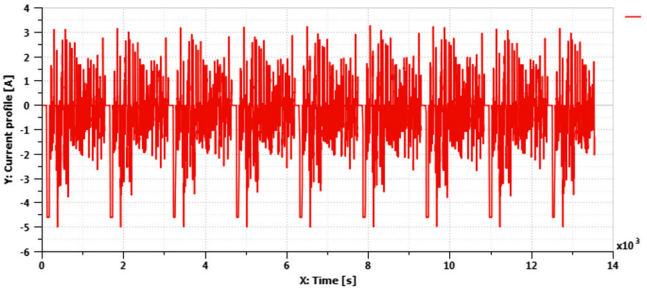

FIGURE 14 Current load profile of UDDS cycles [Colour figure can be viewed at wileyonlinelibrary.com]

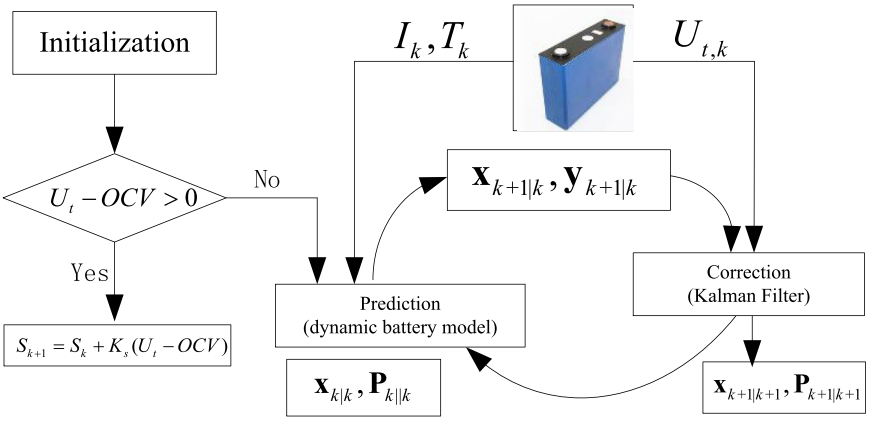

FIGURE 13 The sketch diagram of the SOC estimation based on UKF [Colour figure can be viewed at wileyonlinelibrary.com]

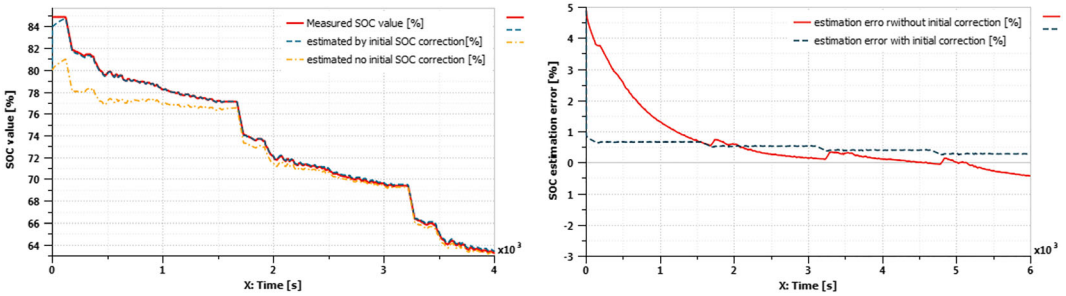

FIGURE 15 Comparison of initial SOC convergence performance and error analysis under UDDS [Colour figure can be viewed at wileyonlinelibrary.com]

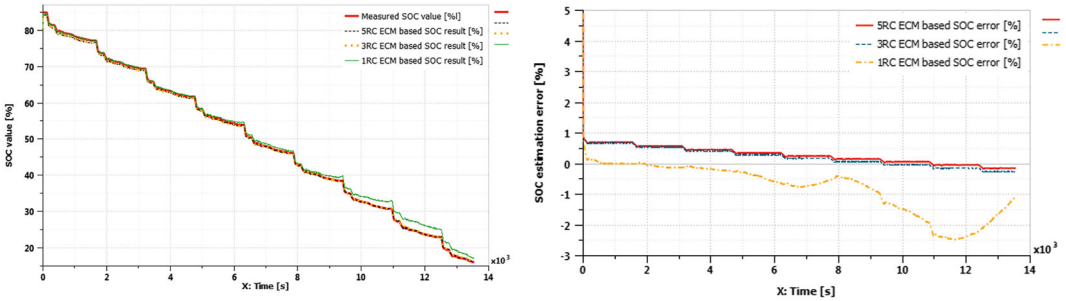

FIGURE 16 Comparison of SOC estimation and errors analysis of three different ECMs under UDDS [Colour figure can be viewed at wileyonlinelibrary.com]

TABLE 3 Model error analysis and calculation time comparison

	1RC Model	3RC Model	5RC Model
Max SOC error, %	1.21	0.69	0.648
Mean SOC error, %	2.74	0.31	0.29
CPU time[a], s	152	161	195

[a]Simulation time is 13 540 s.

ECMs are very similar. But the calculation time is much less than 5RC model and very close to the 1RC-based estimation algorithm.

5 | CONCLUSION

The objective of this paper is to find a better trade-off between battery modeling complexity and modeling accuracy. The terminal voltage and SOC prediction performance of different circuit topologies for diffusion process by using ECMs are studied. The theory of diffusion process approximation by using RC networks is explained in frequency domain combined with battery impedance analyzer. The intrinsic association among EIS equation, transfer function, and R//C equivalent circuit models are explained in the paper. And a novel method of combining UKF and initial SOC correction for SOC estimation is proposed. The results of UDDS show that ECM with three RC networks has the best comprehensive performance on calculation cost and SOC estimation accuracy. And with initial SOC correction method, the convergence speed of SOC estimation is improved significantly.

In the future, the battery aging including calendar and cycling aging of lithium ion batteries will be taken into consideration in SOC prediction to improve the robust performance of SOC estimation algorithm in the whole life cycle of electric vehicle applications.

ACKNOWLEDGEMENTS

This work was in part supported by the National Natural Science Foundation of China (grant no. 51605020) and the National Key R&D Program of China (grant no. 2017YFB0102600).

ORCID

Hongbin Ren https://orcid.org/0000-0002-4903-0935

REFERENCES

1. Wang S, Verbrugge M, Wang JS, Liu P. Multi-parameter battery state estimator based on the adaptive and direct solution of the governing differential equations. *J Power Sources*. 2011;196(20):8735-8741.

2. Montaru M, Pelissier S. Frequency and temporal identification of a Li-ion polymer battery model using fractional impedance. *Oil Gas Sci Dent Tech*. 2009;65(1):67-78.

3. Ren H, Zhao Y, Chen S, et al. Design and implementation of a battery management system with active charge balance based on the SOC and SOH online estimation. *Energy*. 2018;166:908-917.
4. Lai X, Gao W, Zheng Y, et al. Comparative study of global optimization methods for parameter identification of different equivalent circuit models for Li-ion batteries. *Electrochim Acta*. 2019;295:1057-1066.
5. Wang T, Chen S, Ren H, et al. Model-based unscented Kalman filter observer design for lithium-ion battery state of charge estimation. *Int J Energy Res*. 2017;42(2):1-12.
6. Li J, Adewuyi K, Lotfi N, Landers RG, Park J. A single particle model with chemical/mechanical degradation physics for lithium ion battery state of health (SOH) estimation. *Appl Energy*. 2018;212:1178-1190.
7. Xianke L, Xiaoguang H, Andrej I, et al. Physics-based and control-oriented modeling of diffusion-induced stress in Li-ion batteries. *J Electrochem Soc*. 2018;165(10):2255-A2266.
8. Ekström H, Fridholm B, Lindbergh G. Comparison of lumped diffusion models for voltage prediction of a lithium-ion battery cell during dynamic loads. *J Power Sources*. 2018;402:296-300.
9. Wei Z, Zhao J, Ji D, Tseng KJ. A multi-timescale estimator for battery state of charge and capacity dual estimation based on an online identified model. *Appl Energy*. 2017;204:1264-1274.
10. Hafsaoui J, Scordia J, Sellier F, et al. Development of an electrochemical battery model and its parameters identification tool. *Int J Automot Eng*. 2012;3(1):27-33.
11. Zhang C, Allafi W, Dinh Q, et al. Online estimation of battery equivalent circuit model parameters and state of charge using decoupled least squares technique. *Energy*. 2017;142(1):678-688.
12. Duong VH, Bastawrous HA, Lim KC, See KW, Zhang P, Dou SX. Online state of charge and model parameters estimation of the $LiFePO_4$ battery in electric vehicles using multiple adaptive forgetting factors recursive least-squares. *J Power Sources*. 2015;296:215-224.
13. Hu X, Sun F, Zou Y, et al. Online estimation of an electric vehicle lithium-ion battery using recursive least squares with forgetting[C]. American Control Conference. IEEE, 2011.
14. Vyroubal P, Kazda T. Equivalent circuit model parameters extraction for lithium ion batteries using electrochemical impedance spectroscopy. *J Energy Storage*. 2018;15:23-31.
15. Khalid K, Mehdi J, Lucia G. Comparison of Li-ion battery equivalent circuit modelling using impedance analyzer and Bayesian networks. *IET Electr Syst Transp*. 2018;8(3):197-204.
16. Zhang L, Wang L, Hinds G, Lyu C, Zheng J, Li J. Multi-objective optimization of lithium-ion battery model using genetic algorithm approach. *J Power Sources*. 2014;270:367-378.
17. Askarzadeh A, Rezazadeh A. Optimization of PEMFC model parameters with a modified particle swarm optimization. *Int J Energy Res*. 2011;35(14):1258-1265.
18. Oldenburger M, Bedürftig B, Gruhle A, et al. Investigation of the low frequency Warburg impedance of Li-ion cells by frequency domain measurements. *J Energy Storage*. 2019;21:272-280.
19. Mu H, Xiong R, Zheng H, Chang Y, Chen Z. A novel fractional order model-based state-of-charge estimation method for lithium-ion battery. *Appl Energy*. 2017;207:384-393.
20. Plett GL. *Battery Management Systems Volume II: Equivalent-Circuit Methods*. Norwood, MA, USA: Artech House; 2015.
21. Lai X, Zheng Y, Sun T. A comparative study of different equivalent circuit models for estimating state-of-charge of lithium-ion batteries. *Electrochim Acta*. 2018;259(1):566-577.
22. Buller S. Impedance-based simulation models for energy storage devices in advanced automotive applications [D]. thesis, RWTH Aachen, Aachen, Germany, 2003.
23. Kuhn E, Forgez C, Lagonotte P, Friedrich G. Modelling Ni-MH battery using Cauer and Foster structures. *J Power Sources*. 2006;158(2):1490-1497.
24. Ren H, Chen S, Zhao Y, et al. State observer-based sliding mode control for semi-active hydro-pneumatic suspension. *Veh Syst Dyn*. 2016;54(2):1-23.

How to cite this article: Ren H, Zhao Y, Chen S, Yang L. A comparative study of lumped equivalent circuit models of a lithium battery for state of charge prediction. *Int J Energy Res*. 2019;43:7306–7315. https://doi.org/10.1002/er.4759